Annals of Nuclear Energy 112 (2018) 132–142

Contents lists available at ScienceDirect

Annals of Nuclear Energy

journal homepage: www.elsevier.com/locate/anucene

Thermal and fluid analysis of dry cask storage containers over multiple years of service

Yongjia Wu, Jackson Klein, Hanchen Zhou, Lei Zuo *

Department of Mechanical Engineering, Virginia Polytechnic Institute and State University, 635 Prices Fork Road, Blacksburg, VA, 24061, USA

ARTICLE INFO

Article history:
Received 31 July 2017
Received in revised form 29 September 2017
Accepted 6 October 2017
Available online 13 October 2017

Keywords:
CFD
Dry cask storage
Nuclear
Thermoelectric

ABSTRACT

A detailed three-dimensional thermal and fluid analysis of a vertical dry storage cask with a canister containing 32 high-burnup pressurized water reactor (PWR) spent fuel assemblies for a storage of 50 years was carried out using a CFD simulation. The input decay heat value was calculated based on a Westinghouse 17 × 17 PWR fuel assembly using the well validated package ORIGAMI imbedded in SCALE, with a total heat load of 38.44 kW for year 5 and 10.67 kW for year 55. The temperature-dependent and anisotropic thermal properties of the fuel assemblies, filling gas within the canister, and air covering the canister were considered in order to preserve accuracy. A peak temperature of 621.4 K occurred in the upper part of the fuel assemblies for at year 5, deceasing to 423.0 K after 50-year service. The simulation results shed light on the temperature and flow environment within the canister for an operational time of 50 years.

Published by Elsevier Ltd.

1. Introduction

In the nuclear industry, nuclear fuel rods are first stored in pools of water (wet storage) to remove heat from the assemblies and shield from gamma and neutron radiation left over from the production of radioactive nuclides in power generation. After 5 years or so, this fuel is then separated and stored in dry storage canisters for 30–60 years. After that, the fuel with low decay heat will be transported to a final disposal site for long term storage (Ewing, 2015). In the U.S. alone, there were 1500 loaded dry casks in 2010, and the number has been increasing by 200 each year. Since 2011, the close of the permanent nuclear waste disposal site in the Yucca Mountains, Nevada has brought dry storage and nuclear waste to the forefront of consciousness in the USA. Dry cask storage in the future may extend for up to one hundred years, which will bring large changes to the design of existing canisters.

Because of their lengthy use, monitoring of conditions within dry casks is of critical importance, as the temperature of the fuel and humidity within the cask can play a key role in the health of the system, and overall longevity of the storage containers. In fact, thermal analysis of spent nuclear fuel has been identified as high priority by the DOE Nuclear Energy Division (Adkins, 2012) since potential failure mechanisms to the fuel and canisters are dependent on temperature. This offers a unique problem however, as monitoring the cask internals can be very difficult, or indeed impossible due to a real potential for harm from radiation leakage, (Bruno and Ewing, 2006; Hedin, 1997), and for containment rupture. To address this issue, energy harvesting for wireless communication of conditions within canisters has been studied (Carstens, 2013; Carstens et al., 2013). Wireless communication of data from inside the cask would remove the need for human inspection, and energy harvesting could potentially allow for sensors to run indefinitely. Such a system would be able to report, in a self-powered way, information on the fuel and environment within the canister, without the need for operators. To address this, a detailed thermal environment analysis in the canister is necessary in order to guide the placement of a thermoelectric energy harvester. This paper is primarily concerned with a simulation of the thermal performance of a vertical HI-STORM-100 dry storage cask with a MPC-32 canister containing 32 high-burnup (45 GWd/MTU) Pressurized Water Reactor (PWR) spent fuel assemblies (Westinghouse PWR 17 × 17) for a storage of 50 years. This cask is further outlined in Section 2.

Much of the past work studying the thermal environment in canisters has been based on simulation, due to the dangerous nature of conducting in-situ experiments. The gamma radiation flux in the canister is very high, extremely dangerous for human beings, even after long periods of storage (Hedin, 1997). One of the reliable reported in-situ experiments done is in a DOE report from 1992 (McKinnon et al., 1992) where a performance test was done on a Pacific Sierra nuclear VSC-17 ventilated concrete storage dry cask

* Corresponding author.
E-mail address: leizuo@vt.edu (L. Zuo).

https://doi.org/10.1016/j.anucene.2017.10.013
0306-4549/Published by Elsevier Ltd.

configured for PWR fuel assemblies. The comprehensive report described the details of the fuel assembly type and position, geometry configuration of the cask system, material properties of individual components, and filling gas within the canister. The temperature profiles on the cask surface, concrete, air channel surfaces, and fuel canister guide tubes were described in detail, which provided precious data for validation of simulation results. Other experimental work has been done on both full scale and scaled down cask systems with the fuel simulated by electrical heating (Takeda et al., 2008; Wataru et al., 2008). This type of experiment can accurately represent the real cask system, however due to the complexity, simulation may be preferred.

Most thermal analyses of canisters have been done primarily for the purpose of certification, many of which that can be found from the NRC's library (Creer et al., 1987; Holtec International, 2012). Most of this work, since it was used in certification, was conservative because it was used to ensuring a large enough temperature safety margin in the nuclear fuel. In the 80 s, a lot of thermal simulation work for the low burnup fuel can be found for various canisters using COBRA-SFS (Creer et al., 1987; McKinnon et al., 1992; Rector et al., 1986), a CFD code based on the finite volume method. However, the accuracy of the simulation results was undercut by many uncertainties, such as oversimplified energy and momentum equations, and grid systems which were very sparse.

Due to an increase in computational power, from the beginning of this century, more studies have been performed using CFD to ensure spent fuel is maintained below its critical temperature in various cask systems. This trend is driven by the need to design better performing casks which can host more fuel assemblies and high burnout fuels. Early work includes Xie et al. (2002) who simulated a horizontal 2D dry storage system using the PHOENICS package and Greiner et al. (2007) who conducted 2D numerical studies of multipurpose canisters with 21 PWR assemblies and analyzed how nitrogen and helium cover gas, and different fuel cladding emissivity effected the thermal performance for different fuel decay heat generation rates. Wataru et al. (2008) conducted a 3D thermal analysis for the concrete cask using the FIT-3D thermal hydraulics code and the commercial PHOENICS package. Their computed temperature values and air flow velocities were validated by comparing with experimental data presented by Takeda et al. (2008). Results showed that the CFD approach can provide reasonable temperature estimates for the canisters. Lee et al. (2009) presented a thermal-fluid flow analysis of a vertical dry cask storage system under normal and off-normal conditions using the commercial CFD code, FLUENT. An effective thermal conductivity approach and a porous media approximation was used to model the fuel rods. The temperature and flow velocity profiles in the canister were compared and verified by the thermal test results collected from a half scaled-down model. A lot of CFD work (Das et al., 2010; Li and Liu, 2016; Walavalkar and Schowalter, 2004; Zigh and Solis., 2012) was done to analyze the VSC–17 cask system because the experimental result for this canister was well documented in the 1992 DOE report (McKinnon et al., 1992) mentioned earlier. Walavalkar and Schowalter (Walavalkar and Schowalter, 2004) performed a 3D CFD analysis for a 90-degree section of VSC–17 spent fuel dry storage system using the FLUENT software. They found the CFD simulation result can accurately predict the thermal environment in the VSC–17 spent fuel dry storage system. Work done by Zigh and Solis. (2012) and Das et al. (2010) further demonstrated that the excellent performance of CFD in calculating the temperature and flow velocity in the dry cask. In all of these studies, however, approximations were often used for the conditions inside and outside of the cask, largely due to missing, and difficult to acquire experimental data. Estimations were generally made on: the decay heat generated by the fuel, the distribution of the heat in the fuel assemblies, the thermal properties of both the backfilled helium and steel basket in the MPC, and the thermal properties of the fuel assembly itself.

These unnecessary assumptions and estimations undercut the accuracy of the CFD work. It is evident upon study of these previous works that the heat load applied to the inside of the dry cask in order to simulate the decay heat generated by the spent fuel was somewhat arbitrary and are generally only given as one set value, typically estimated from other work or experimental analysis from many years ago. Recently, Li and Liu (2016) established a 3D model of a vertical dry cask to simulate a vertical storage cask containing a welded canister with 32 Pressurized Water Reactor (PWR) used-fuel assemblies, with a total decay heat load of 34 kW by using the ANSYS/FLUENT code. Their work was performed in order to study the effects in changes of the thermal conductivity of the basket, and of the pressure and makeup of the gas backfilling the MPC canister. Herranz et al. (2015) took data from the Holtec International manual (Holtec International, 2004, 2010) for design of MPC-32, and placed a total heat power of 30 kW in the fuel assemblies, in order to study the sensitivity of maximum fuel temperature to heat load distribution within the canister, cask design (inlet/outlet orientation) and local environmental temperatures.

Much work, however, has been done previously characterizing the distribution of heat along the fuel assemblies (McKinnon et al., 1992; Turner, 1989; Zigh and Solis., 2012), as well as the effective conductivity of the fuel assemblies as a function of temperature within the cask (Bahney and Lotz, 1996; Mittal et al., 2014). Yoo et al. (2010) simulated thermal behaviors of the TN24P cask without a concrete wall. With a geometrical model resolution down to each individual fuel pin level, the simulation did not need to introduce effective thermal conductivity for the fuel assemblies. The heat load applied to their work was the same as estimated by the experiment (Creer et al., 1987), at 20.6 kW in the total cask. Their work was found to agree very well with the reported experimental results. Brewster et al. (2012) demonstrated a simulation on a TN-24P cask with geometry resolution down to each individual fuel and its cladding level. The calculation was carried out on a half-cask scaled model with a grid number up to 42.9 million using a STAR-CCM+ CFD code. This model was found to be more accurate in predicting the peak cladding temperatures (PCTs) when compared with the traditional porous media/effective thermal conductivity approach.

Though the CFD models listed above used for canister simulation have progressed a lot in the past decade, there are still some gaps that need to be filled before this technology can be used to accurately predict the temperature and guide the design of new canisters. While these studies take into consideration many aspects of the dry storage canister, they do not consider precise calculations of the state of the spent fuel upon entering the dry cask canister, nor do they take into account the varying heat load of the spent fuel during its lifetime. Considering the fact that decay heat of the fuel will change throughout the lifetime of the cask due to decreasing activity (or decay) of isotopes present, thermal analysis of the dry cask storage system should reflect this. Precise calculation of both the decay heat present, and its variability with time is generally left out of the literature, and thus it is evident that more work is needed in the area of thermal simulation for dry cask storage. In this work, ORIGAMI (Williams et al., 2015) is used in order to model the decay heat present in the canister at the time of storage, and throughout 50 years of life within the canister. This was done to provide a very accurate approximation of the actual heat load in the canister for a common Westinghouse 17 $\times$ 17 fuel assembly with an initial enrichment of 4.5% and a burnup of 45 GWd/MTU.

To better improve the accuracy of the simulation result and guide the future canister design, the present paper introduces an improved model for thermal-fluid dynamic simulations of an

MPC-32 dry cask. Built on approaches well validated in previous 3D CFD studies, some new approximations are adopted to improve the accuracy of the simulation, making it closer to real dry cask systems. First, temperature-dependent and anisotropic thermal properties of the fuel assemblies, filling gas, and air are introduced in order to preserve accuracy while overcoming drawbacks associated to traditional estimations. Second, in some of the previous literature, the filling gas was assumed to be steady and only conduction was considered (Das et al., 2010), which might cause the overestimation of the overall temperature within the canister. In this work, both the convective flows inside and outside the MPC were considered, which can significantly accelerate the heat transfer process. In addition to this, after examining the Reynolds number within the air gap, it was found to be in the transitional, thus turbulence modeling is also considered in this work. Last but not the least, the input decay heat value is not taken as randomly assigned value, as has been done extensively in the CFD analyses in the literature, but calculated based on a Westinghouse 17 × 17 fuel assembly using the well validated package ORIGAMI imbedded in SCALE. The thermal analysis made in this work will be used to guide the design a self-powered ultrasonic wireless monitoring system for the canister which can sense and monitor temperature, pressure, and moisture for the first 50-years life of this cask, and thus analysis is given on the potential for energy harvesting within the dry cask. Ultimately, this work addresses some issues in the CFD modeling of canister, and provides comprehensive and acceptable thermal-fluid dynamic data to guide both future canister designs and thermal energy harvesting for wireless sensors within MPCs.

2. Dry cask mathematical model

2.1. SCALE decay heat calculation

ORIGAMI, a part of the SCALE Code System from ORNL, is widely used in the nuclear industry in order to calculate the isotopes present after various conditions are applied to a type of nuclear fuel. The software can accurately perform isotopic depletion and decay heat calculations for a wide range of fuel assemblies. In this work, the software was used to calculate the decay heat and nuclide makeup for the fuel under consideration from the time it left the reactor, to 50 years in dry cask storage (55 years since removal). In this way the decay heat in the CFD analysis can be tailored to the specific fuel and time frame desired for simulation.

The fuel employed for the simulation here was a Westinghouse 17 × 17 assembly, with a total cask MTU of 15 spread over the 32 assemblies, an enrichment weight percentage of U235 of 4%, a burnup of 45 GWd/MTU, 3 runs per fuel assembly, and an average power of 40 MW/MTU. This fuel configuration approximates an average assembly being removed from a reactor, as typical fuel now has a U235 enrichment between 3 and 5%, and is used up to, and in the future past, 45 GWd/MTU (Bruno and Ewing, 2006). Using this average fuel allows one to get a typical decay heat magnitude and trend. A more accurate representation of an actual fuel assembly can be made by inputting the data taken from a reactor history if desired, however as this data is highly specific to the reactor and fuel assembly, a general route was taken by the authors in order to show the process, and to show the characteristics of an average set of fuel.

ORIGAMI offers an "Express form" (Williams et al., 2015) which was used by the authors, and can be used to quickly perform decay calculations on typical assembly types given limited knowledge of the fuel and reactor. A more rigorous analysis can be done if actual data from a reactor is retrieved, and the results are desired. The calculations for decay heat were taken using this express form, and the parameters listed above. It is assumed the power reactor contained 90 MTU and the fuel is evenly distributed among 193 fuel assemblies. Based on this, the watts per assembly can be determined (Carstens, 2013). The total power of the MPC-32 along with the associated gamma and neutron intensities at various years throughout the lifetime of the cask, starting from 5 years after removal from the reactor, at the start of dry storage, and finishing with 55 years, at the 50-years mark for dry storage, are illustrated in Table. 1.

The decay heat generated within the dry cask storage is highly dependent on the fuel makeup, and its operation within the reactor. As shown in table 1, it also depends on how long the fuel has been stored. This process of calculating the decay heat can be used to get a very precise approximation of the heat generated when placed into dry cask storage. The total decay heat is then assigned to each fuel assembly according to a ratio of X ($X = 9/11$ in this paper) described below (Fig. 1).

2.2. Thermal-fluid modeling

2.2.1. Conceptual principles

As mentioned above, typical dry casks (Holtec International, 2010), as depicted in Fig. 2, are made up of a thick concrete overpack, and an internal MPC which can hold a variety of different fuels and assemblies inside the metal basket, ranging from 24 to 62 assemblies. The carbon steel basket and wall of the MPC, and the concrete overpack are meant to contain the radiation, while removing heat from the fuel in order to ensure it does not reach a criticality point. This work focuses on a specific canister, an MPC-32 canister made by Holtec International (Holtec International, 2010). The concrete overpack (HI-STORM 100) is made to house the MPC and has inner channels to allow air to flow between the concrete and MPC, cooling the canister by taking advantage of the buoyancy force. Inside the MPC, a steel basket is used to hold the assemblies. The canister is also backfilled with helium to 3.3 atm in order to aid in the conduction and convection of heat away from assemblies, and give an inert gas environment. Decay heat generated by the spent fuel is transferred through the containment wall of the MPC to a cooling air flow. Natural circulation drives the cooling air flow through an annular path between the MPC and the concrete overpack and carries the heat to the environment. The dimension of the canister and overpack are shown in Table 2. To simplify the simulation, the support structures and some small components are neglected.

2.2.2. Mathematical model

Reynolds and Grashof numbers are widely used to judge the flow regime for buoyancy force driven flow. According to the literature (Bejan, 2013), the approximated fully developed velocity pro-

Table 1
Decay heat, gamma intensity, and neutron intensity from the 15 MTUs of spent fuel for 50 years of dry cask storage.

Year (Since removal)	Decay Heat (kW)	Gamma Intensity (#/s)	Neutron Intensity (#/s)
5	38.44	2.64×10^{17}	1.02×10^{10}
10	24.52	1.47×10^{17}	8.4×10^{9}
15	21.07	1.20×10^{17}	7.0×10^{9}
20	19.00	1.04×10^{17}	5.9×10^{9}
25	17.31	9.2×10^{16}	4.9×10^{9}
30	15.85	8.2×10^{16}	4.1×10^{9}
35	14.56	7.3×10^{16}	3.4×10^{9}
40	13.42	6.5×10^{16}	2.9×10^{9}
45	12.40	5.8×10^{16}	2.4×10^{9}
50	11.49	5.1×10^{16}	2.0×10^{9}
55	10.67	4.6×10^{16}	1.7×10^{9}

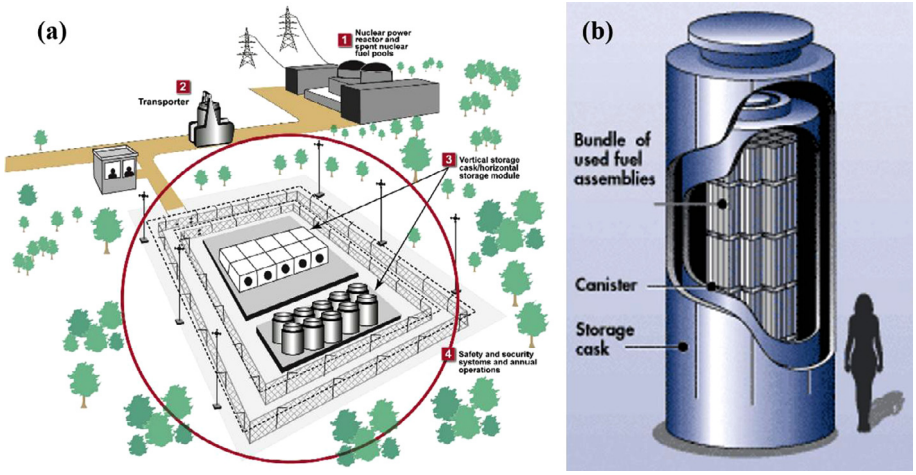

Fig. 1. Depiction of dry cask storage where (a) nuclear waste storage at the at sites where it is generated (U.S. Government Accountability Office, 2017) is shown along with (b) a cutaway of the dry storage canister (United States Nuclear Regulatory Commission, 2017).

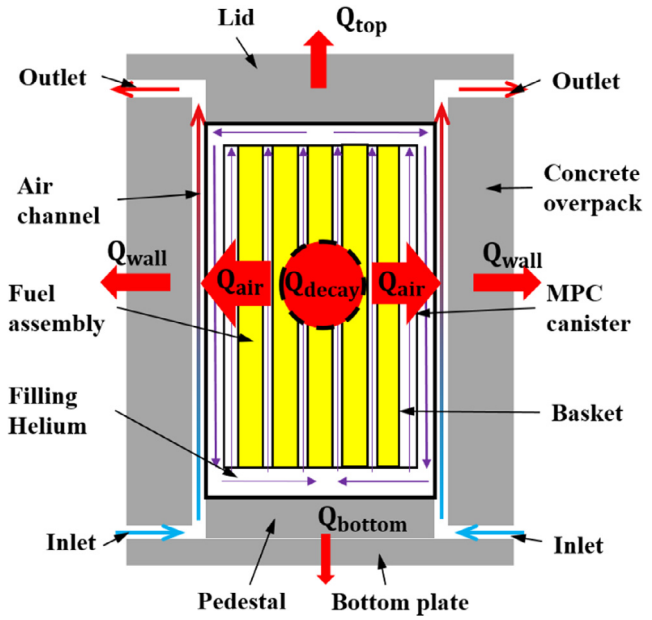

Fig. 2. Model of the Holtec International dry cask canister.

file in the air channel between the MPC and the concrete overpack can be described as

$$v = \frac{g\beta D^2 (T_0 - T_\infty)}{8\nu}\left[1 - \left(\frac{x}{D/2}\right)^2\right] \quad (2)$$

where β is the expansion coefficient, D is the characteristic length (width of the air channel), T_0 is the wall temperature, and T_∞ is the environmental temperature. A rough calculation of the Reynolds number shows that, in this region around the MPC, the Reynolds number is higher than 3000 based on the channel hydraulic diameter and maximum air velocity in the annulus, which is clearly above the critical Reynolds number of 2300 for internal flows. Thus we judge that the air flow is in a transitional range between the laminar and turbulent regimes. This is different from Zigh and Solis. (2012) who mentioned that the air flow can be a laminar flow based on Grashof number, another criterion proposed by Sparrow and Azevedo (1985).

Table 2
The main dimensions of the Holtec HI-STORM 100 overpack and MPC-32 canister.

HI-STORM 100 overpack (m)		
Concrete	Height	6.09
	Radius outer	1.68
	Radius inner	0.98
Inlet vent	Height	0.25
	Width	0.38
Outlet vent	Height	0.15
	Width	0.64
Pedestal	Height	0.64
	Radius	0.89
MPC-32 canister (m)		
Shell	Height outer	4.85
	Height inner	4.50
	Radius outer	0.89
	Thickness	0.013
Basket	Thickness	0.0096
	Basket Cell inner	0.224 × 0.224 × 3.66
Lid	Thickness	0.29
Westinghouse 17 × 17 fuel assembly (m)		
Fuel	Fuel Cell	0.214 × 0.214
	Active length	0.366

Table 3
Thermal properties of the helium and air.

Helium	
Thermal conductivity (W/m·K)	0.0383 + 4.1713e−4·T −1.0193e−7·T^2
Density (kg/m^3)	0.4875
Viscosity (kg/(s·m)	1.84e−5
Expansion coefficient (1/K)	0.002
Air	
Thermal conductivity (W/m·K)	−5.22e-5 + 9.78e−5·T-3.39e−8·T^2
Density (kg/m^3)	1.00
Viscosity (kg/(s·m)	1.79e-05
Expansion coefficient (1/K)	0.00283

On the other hand, the helium flow inside the canister is predicted to be in the laminar regime based on the Reynolds and Grashof numbers. Here, the temperature increase of the air flow is less than 70 K, thus $\beta(T - T_0) \ll 1$, so Boussinesq approximation can be used to calculate the buoyancy force without significant derivation.

The Reynolds time-averaged k-ε turbulence model with standard wall functions and transitional SST k-ω are used to model turbulence in the air channel and canister. The k-ε turbulence model with standard wall functions can predict the fluid behavior of fully

developed turbulence flows with fairly high accuracy, as has been well validated by the industrial community in the past 30 years. On the other hand, the transitional SST k-ω is the most general turbulence model. The transitional SST k-ω model initially attracted attention because it does not require wall-damping functions for low Reynolds number applications. By introducing blending functions, this model combines the good near-wall behavior of the k–ω model with the robustness of the k–ε model in the far field in a numerically stable way. The governing equations (Versteeg and Malalasekera, 2007) of the transitional SST k-ω model are prescribed by

Continuity equation

$$\frac{\partial(\rho)}{\partial t}+\frac{\partial(\rho u_j)}{\partial x_j}=0 \tag{3}$$

Momentum equations

$$\frac{\partial(\rho u_i)}{\partial t}+\frac{\partial(\rho u_i u_j)}{\partial x_j}=\rho g\beta(T-T_\infty)-\frac{\partial p}{\partial x_i}+\frac{\partial \tau_{ij}}{\partial x_j}+\frac{\partial}{\partial x_j}\left(\eta\frac{\partial u_i}{\partial x_j}\right) \tag{4}$$

where $\tau_{ij}=-\rho\overline{u_i'u_j'}=2\mu_t S_{ij}$, S_{ij} is the mean rate of strain tensor.

Energy equation

$$\frac{\partial(\rho c_p T)}{\partial t}+\frac{\partial(\rho c_p u_j T)}{\partial x_j}=\frac{\partial}{\partial x_j}\left(\lambda\frac{\partial T}{\partial x_j}\right)-\tau_{ij}\frac{\partial u_i}{\partial x_j}+\beta T\left(\frac{\partial p}{\partial x_j}+u_j\frac{\partial p}{\partial x_j}\right)+S_i \tag{5}$$

The k equation

$$\frac{\partial(\rho k)}{\partial t}+\frac{\partial(\rho k u_j)}{\partial x_j}=\frac{\partial\left(\left(\mu+\frac{\mu_t}{\sigma_k}\right)\frac{\partial k}{\partial x_i}\right)}{\partial x_j}+\left(\tau_{ij}\cdot S_{ij}-\frac{2}{3}\rho k\frac{\partial u_i}{\partial x_j}\delta_{ij}\right)-\beta^*\rho k\omega \tag{6}$$

The ω equation

$$\begin{aligned}\frac{\partial(\rho\omega)}{\partial t}+\frac{\partial(\rho\omega u_j)}{\partial x_j}=&\frac{\partial\left(\left(\mu+\frac{\mu_t}{\sigma_\omega}\right)\frac{\partial\omega}{\partial x_i}\right)}{\partial x_j}\\&+\gamma_2\left(2\rho S_{ij}\cdot S_{ij}-\frac{2}{3}\rho\omega\frac{\partial u_i}{\partial x_j}\delta_{ij}\right)-\beta_2\rho\omega^2\\&+2\frac{\rho}{\sigma_{\omega,2}\omega}\frac{\partial k}{\partial x_k}\frac{\partial\omega}{\partial x_k}\end{aligned} \tag{7}$$

where the σ_k, β^*, $\sigma_{\omega,2}$, γ_2 and β_2 are revised constants, with the corresponding values 2.0, 0.009, 1.17, 0.44, and 0.083, respectively. μ_t and σ_ω are related to the blending functions to make the equations suitable for both the low and high Reynolds numbers flow regions.

The Discrete Ordinates (DO) Radiation Model is used to model the thermal radiation in the cask. This model is selected because it spans the entire range of optical thicknesses, and allows for problems to be solved with surface-to-surface radiation. Four angular discretization steps are used in each direction of the spherical coordinates system to insure reasonable accuracy.

The CFD analysis of the cask storage system is carried out using the ANSYS/FLUENT 14.0 package. A 90-degree section of the MPC–32 spent fuel dry storage system, shown in Fig. 3, is employed for the simulation. Two grid systems with 1,814,658 and 4,442,080 hexahedral grids are used. The dimensionless distance (y+) between the wall and the cell center of the near wall grid for the first mesh is around 20. To better improve the performance of the transitional k-ω SST model at the near wall viscosity-affected region, the grids near the canister wall is refined in order to let y +$\sim$1(with grids number increases to 4,482,080). The grid quality is well checked to ensure better convergence. The simulation on the year 5 case finds no significant difference on the outlet air volume flow rate for these two grid system. Thus, the grid system with 4,442,080/4,482,080 hexahedral nodes is used to do the case by case calculations. The SIMPLE algorithm is used to solve the Navier–Stokes equations in a segregated manner. A body-force-weighted scheme is used for the pressure discretization, as the buoyancy force acts as the driving force. The discretization method used for all the other parameters is the second-order upwind method. The iteration continues until the residuals are less than 10^{-3} for the mass, momentum, and turbulence equations, and 10^{-6} for the k, ω and ε energy equations. A second criterion to check the convergence of the iteration is to monitor the volumetric flow rate of the air flow at the vent outlet. When the fluctuation is less than 1.0%, the iteration can be regarded as converged.

2.2.3. Decay heat in the fuel assembly

In some previous literature, the heat load was assumed to be uniformly distributed in the fuel assembly. In the real case, the heat load varies in both the radial and axial directions. The heat load distribution in the fuel assembly is known to be a key element in determining the real temperature profiles within the canister (Herranz et al., 2015; Holtec International, 2010). Generally, the fuel assembly positions in the MPC basket honeycomb (Fig.4a) can be grouped in two regions: the inner one (orange), with a number of 16 cells, and the outer one (yellow), with a total of 16 cells. The fuel assemblies in the same region are assumed to have the same load heat. To better simulate the real system, a more precise heat load function can be fit. The relation between the actual heat load (Q) and the designed one (Q_{des}) is a function of X (Herranz et al., 2015),

$$Q(X)=2\frac{Q_{des}}{1+X^{0.23/X^{0.1}}} \tag{8}$$

where X is the ratio between inner and outer heat loads of fuel assemblies. For our case, the total heat load between the outer and inner fuel assembly are set to be 9/11.

According to Turner (Turner, 1989) the load heat for in a single fuel assembly is non-uniform shown in Fig.4b. The cross-section edge is very much smaller than the length of the fuel assembly, thus it is reasonable to assume a uniform heat generation rate on the cross-section. However, a peaking factor profile for the heat generation rate along the axial length of the fuel assembly is adopted to improve the simulation accuracy.

$$\begin{aligned}q_{load}=1.1A\cdot(&0.0237\cdot Z^5-0.3287\cdot Z^4+1.5058\cdot Z^3\\&-2.9965\cdot Z^2+2.6204\cdot Z+0.3927)\end{aligned} \tag{9}$$

where the A is adapted according to each case to ensure the total load heat is equal to the total assigned heat load calculated from ORIGAMI. Numerical implementation of the distributed load heat is achieved by using the User Defined Functions (UDFs) embedded in FLUENT.

2.2.4. Material properties

The thermal properties of the materials, including the density, thermal conductivity, heat capacity, viscosity, thermal expansion coefficient, and surface emissivity, are obtained from literature (Mittal et al., 2014; Zigh and Solis., 2012). Among all these properties, special attention should be paid to the thermal conductivity of the air and the fuel assembly. As the air takes away more than 80% of the total decay heat, a small change in the air properties will introduce significant influence on the temperature profile in the fuel assembly.

2.2.4.1. The fuel assembly. In these simulations, the thermal conductivities were assumed to be constant for each of the solid components, except the fuel assembly. The physical properties of canister/cask components were obtained from the Safety Analysis

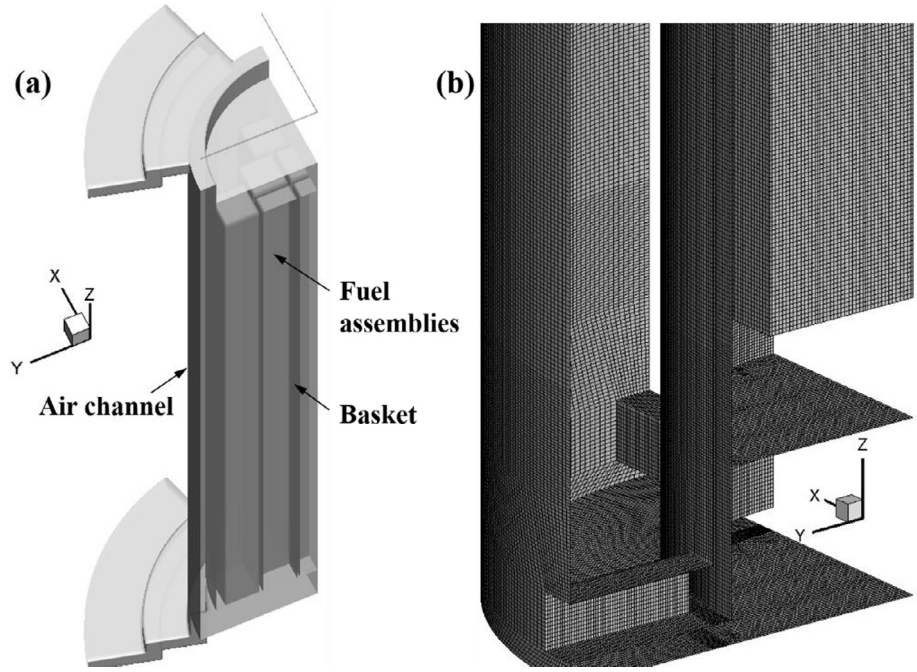

Fig. 3. Holtec International dry cask canister: (a) Internal structure of the dry cask system; (b) the grid system.

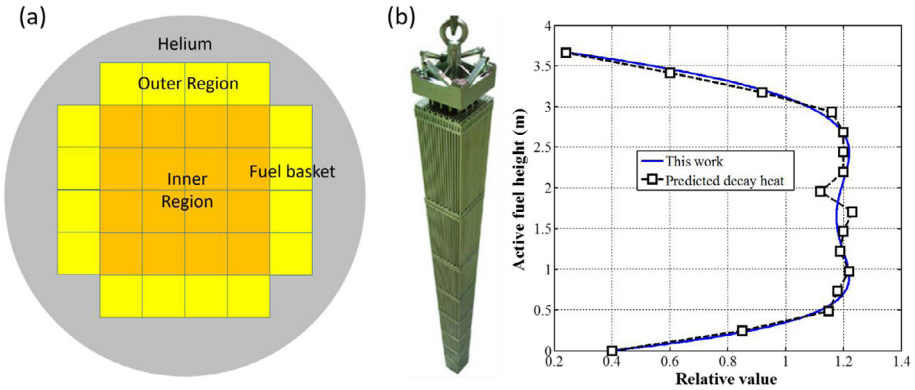

Fig. 4. The load heat distribution in the fuel assembly: (a) Load heat distribution in radial direction; (b) Load heat distribution in axial direction of the fuel assembly (World Nuclear Association, 2017).

Report for the HI-STORM 100 Cask System (Holtec International, 2010).

The spent nuclear fuel generates heat as a result of continuing isotope decay resulting in gamma and neutron generation. All heat generated within the fuel rods will be rejected into the environment through the parallel heat transfer process combining the conductivity and convective heat transfer of the filling gas (helium), and thermal radiation. It is computationally cost expensive to model the details of every fuel rod in the stored fuel assemblies. In a fuel assembly, the fuel rods are arranged neatly, making it accurate and economic to characterize the anisotropic conduction media using an effective thermal conductivity method. A 2D model of a Westinghouse 17 × 17 Standard PWR spent fuel assembly was constructed to determine the planar effective thermal conductivity (k_{eff}) of the spent fuel assembly by Mittal et al. (2014), following the k_{eff} methodology described in the TRW report (Bahney and Lotz, 1996) by Bahney and Lotz. The in-plane thermal conductivity and the axial conductivity of the fuel region with a filling gas of helium are illustrated by Fig. 5. It should be noted that this method will be accurate enough to catch the main characterization of the

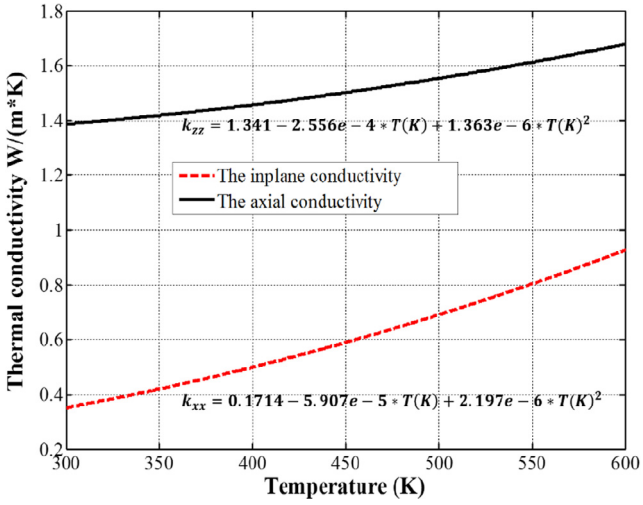

Fig. 5. The in-plane thermal conductivity and the axial conductivity of the fuel region with a filling gas of helium.

thermal and flow information, but might lost some accuracy to predict the peak temperature within the system.

2.2.4.2. The helium and air properties. The helium gas (Table 3) is used to fill the MPC, enhancing the convective and conductive heat transfer between the basket and the canister shell. In these simulations, the pressure is set to be 3.3 atm with corresponding gas properties taken from literature (Tallackson, 1976). The ambient pressure outside the cask was assumed to be 1.0 atm. The thermal conductivity of the air (Table 3) is temperature dependent in this simulation, since the air flow plays a key role in the heat dissipation. With a temperature increase from 294.15 K to 364.15 K, the thermal conductivity of the air increases nearly 20%, which might significantly influence the final result.

2.2.5. Boundary conditions

The boundary conditions below in table 4 used in the CFD model are the same as used in references (Zigh and Solis., 2012), and (Li and Liu, 2016). These coefficients are calculated based on free convection correlation in still air for vertical and horizontal surfaces. At the bottom surface of the cask, equivalent resistance of heat conduction to underlying soil is used to prescribe an equivalent heat transfer coefficient. The emissivity of all the internal surfaces are set to be 1.0 for simplification.

3. Simulation results

The thermal-fluid dynamic performance of the HI-STORM 100 cask and MCP-32 canister system has been explored under steady state conditions. The temperature and velocity profiles within the system are of primary concern in the development of a TEG energy harvester to power the wireless sensors, and thus are outlined below.

3.1. Temperature profiles

Fig. 6 below shows the temperature contours for the vertical storage cask with a helium-filled (3 atm) canister and a stainless steel basket holding 32 spent fuel assemblies with a total heat load of 38.44 kW for year 5 (beginning of dry cask storage), and 10.67 kW for year 55 (50 years of dry cask storage) in Fig. 7. A peak temperature of 621.4 K occurs in the upper part of the fuel assemblies for at year 5.

When comparing these results with other work which assumes that the helium gas is steady and only conductive heat transfer is considered, the peak temperature point in this work shifts significantly to a higher position within the fuel assemblies. This can be reasoned by a helium cycling phenomenon caused by the buoyancy force generated within the canister. On one hand, the helium filling the gap between the basket and the fuel assembly is heated through the convective and conductive heat transfer process. On the other hand, the helium outside the basket is cooled down by the relative cold MPC wall. The buoyancy force aroused by the variation of the helium density drives the natural circulation flow within the canister, which enhanced the thermal performance of the canister. This phenomenon is more obvious for the cases with younger spent fuels, due to the more intensified helium circulation. This cooling process is also reflected in the relative low temperature at the surface of the fuel assemblies. As expected, the overall temperature of the dry cask system decreased gradually with time. After 50-years operation, the peak temperature is about 436.0 K, which is far below the temperature safety margin.

Table 4
Boundary conditions for the CFD simulation.

Parameters	Value
Ambient temperature (K)	294.15 K
Inlet pressure (atm)	1.0
Outlet pressure (atm)	1.0
Heat transfer coefficient on the top and at the side of the dry cask (W/(m^2·K))	5.0
Heat transfer coefficient on the bottom surface (W/(m^2·K))	0.17
Soil temperature	288.15 K
Pressure in the canister (atm)	3.0
Vertical cross-sections	Symmetric

The thermal environmental information is extracted from the CFD simulation result to guide an energy harvester design. It may be possible to install a TEG energy harvester above the fuel assembly, or near the vertical wall of the canister. Fig. 8 below gives the radial temperature profile at Z = 3.19 m at the center (axially) of the cask. It is found that both the k-ε and transitional SST k-ω model can reasonably predict the temperature field, as the temperature profiles obtained by these two models are similar to each other. Actually, to power a 1.0 W sensing and data transmission for 3 s every 5 min, we only need 10 mW of continuous power from an energy harvester. For the year 5 case, the temperature drop near to the canister wall is as high as 70 K, which is more than enough for high performance TEG to harvest enough energy for sensor network powering. However, for year 55 case, the temperature drop is only about 13 K. To generate enough energy, like 10 mW we estimate, the TEG energy harvester should be carefully designed to meet the goal.

Another position may show promise for the TEG energy harvester installation is space somewhere above the fuel assembly. Thus the thermal profile of the canister was also taken axially along the MPC wall, as shown below in Fig. 9. Because of the thermal radiation heat exchanged between the top surface of the fuel assembly and the top wall of the canister, there is a temperature jump at the canister surface, where the wall temperature was slightly higher than the helium gas near the wall. At year 5, the temperature difference near the canister wall is about 20 K, which reduces to ~5 K at year 55. Thus it would be challenging to install a successful energy harvester at this location.

Because of the air channel and the thick concrete wall, the temperature outside the canister is relatively low, as is presented below in Fig. 10. A rough calculation finds that less than 20% of the total heat is dissipated into the environment through the outer wall of the dry cask. The concrete outer surface temperature increases with the height, appropriately considering the heat distribution in the fuel and the air flow along the inner surface of the overpack. At the top end of the concrete surface, somewhere near the outlet of the air channel, the temperature reaches the peak value. Considering the temperature difference between the wall and ambient (295.15 K) is more than 20 K even for the year 55 case, it is possible to build an independent TEG energy harvester to power smart sensors for concrete structural health monitoring.

3.2. Airflow profiles and properties

The flow regions within the dry cask system can be divided into two regions, with their thermal boundary coupled at the canister wall as shown below in Figs. 11 and 14. Inside the canister, there is a flow circulation driven by the buoyancy forces caused by the temperature difference between the core of the fuel assembly and the canister wall. Outside the canister, another flow is aroused by the stack effect cooling down the canister wall effectively. The CFD analysis finds that the peak speed of the flow within the canister occurs near the canister wall, with another sub-peak near the basket wall. For the year 5 case, the flow speed is as high as 0.3 m/s near the MCP wall. After 55-years storage, the flow speed is still as

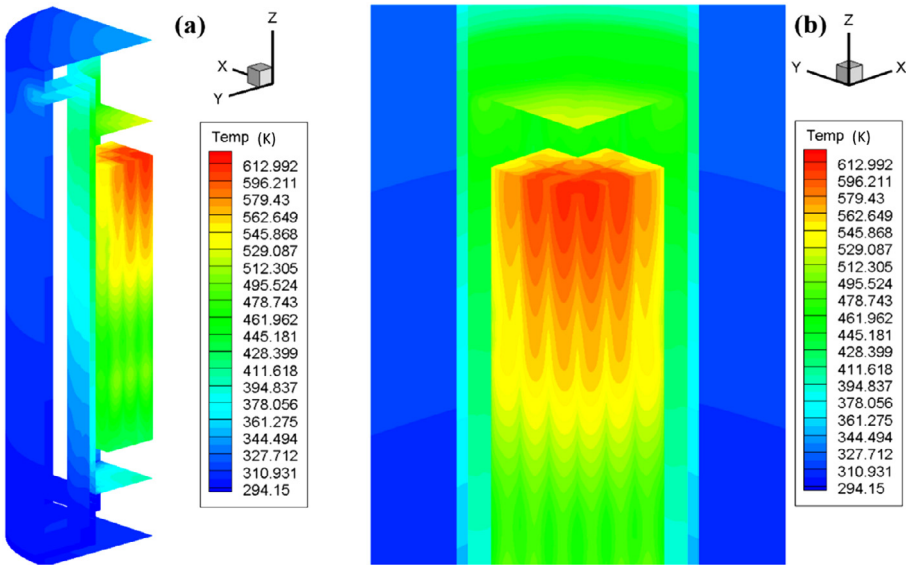

Fig. 6. The temperature profiles in the canister at years 5 after the fuel removed from the reactor using the transitional SST k-ω turbulence model.

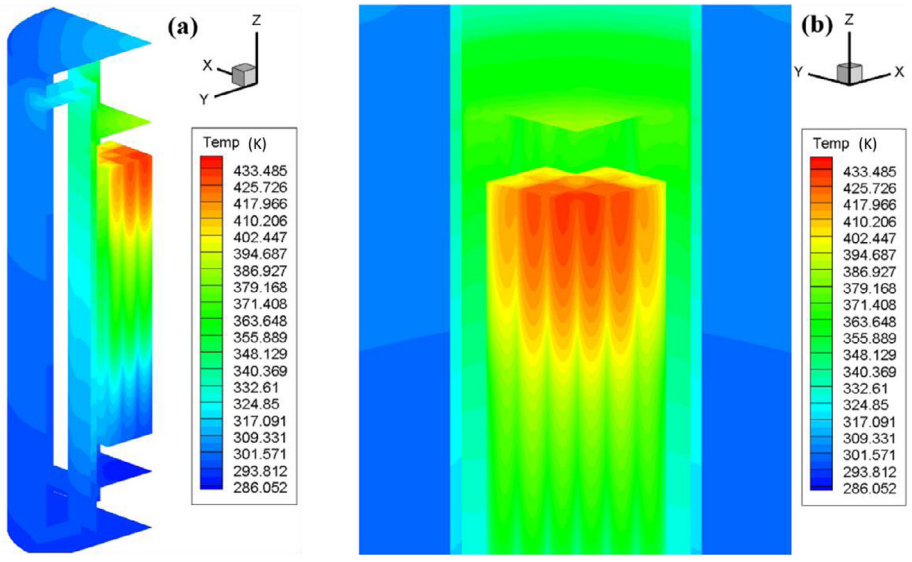

Fig. 7. The temperature profiles in the canister at years 55 after the fuel removed from the reactor using the transitional SST k-ω turbulence model.

high as 0.15 m/s. A TEG energy harvester might take advantage of the low speed flow to enhance its performance.

Outside the MPC within the air channels, we can identify two buoyancy driven natural convections near to the walls characterized as the two relative maxima in Fig. 11. Importantly, the two velocity profiles driven by these two natural convection sections do not converge, which implies the flow here at a height of Z = 3.19 m, the center of the cask, is still not fully developed. This shows that the k-ε model is less valid for turbulence modeling in the dry cask system.

The average flow temperature and volumetric flow rate within the air channel are illustrated in Fig. 12, and can be seen to decrease gradually over time. The average temperature of the hot air is about 352 K at the beginning of dry cask storage, and decreases to 319 K after 50-years operation. At the same time, the flow volume rate decreases from 0.102 $(\times 4)$ m^3/s to 0.065 $(\times 4)$ m^3/s. The thermal energy dissipated through the air channel can be calculated by $q = \dot{m} c_p \Delta T$. Thus, based on the simulation result, more than 80% of the total decay heat is rejected into the environment through the air convection process.

3.3. Validation

To validate the accuracy of the fluid model, the simulation result is compared with the experimental data documented in reference (Waldrop and Kessler, 2014). In their report the total decay heat is 25.2 KW, a value close to year 10 in this scenario, and the ambient temperature is 293.15 K. The calculated temperatures along the vertical wall of the MPC at the symmetric surface are plotted in Fig. 13 along with the data measured by Waldrop and Kessler (2014) at Diablo Canyon and the simulation results obtained by Li and Liu (2016). Temperature measurements are performed at Diablo Canyon with thermocouples inserted from one of the air exit vents at the top of the cask. The simulation results

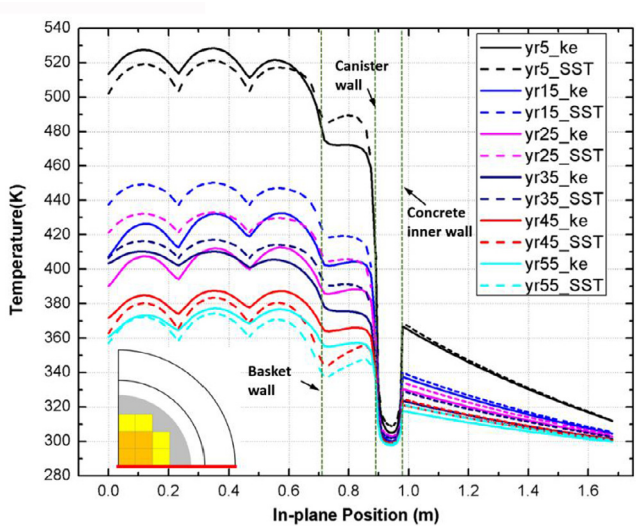

Fig. 8. The radial temperature profile at Z=3.19 m at the symmetry surface.

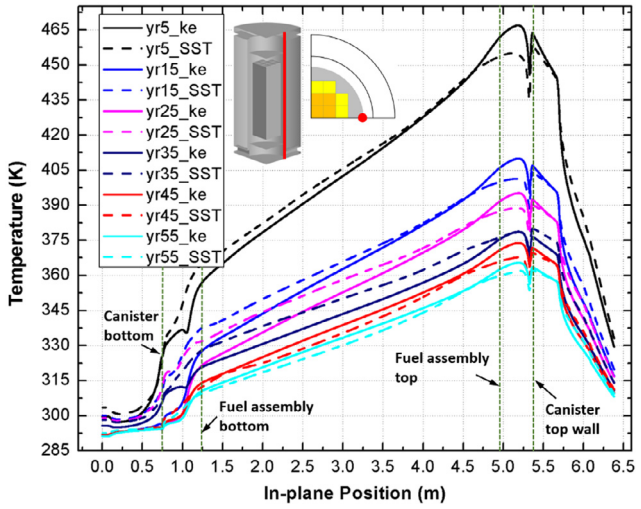

Fig. 9. The temperature profile along the outer surface of the canister.

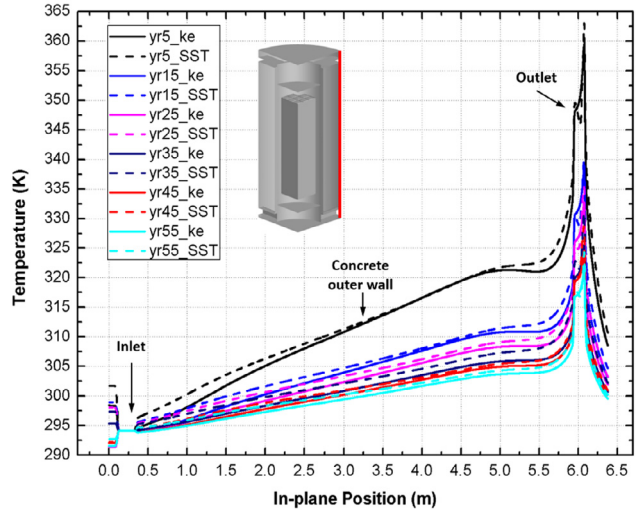

Fig. 10. The temperature profile along the outer surface of the canister.

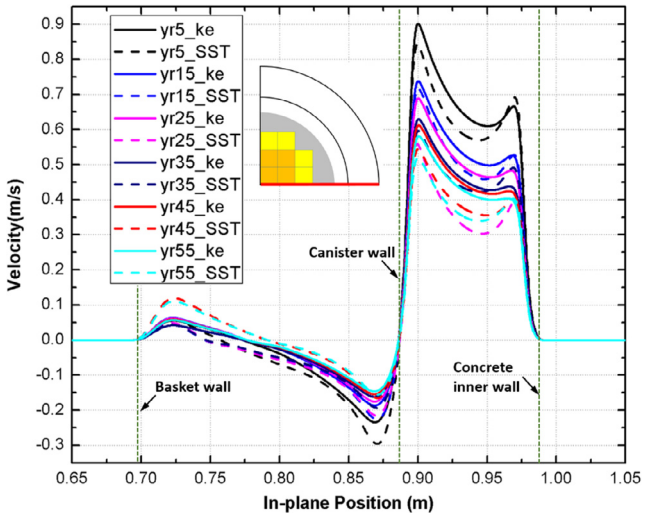

Fig. 11. The radial flow velocity profile at Z=3.19 m in the symmetry surface.

agree well with each other, while both of them deviate from the experimental result, especially at the top end of the MPC wall. This may be caused by the turbulence model we selected over predicting the convective heat transfer at the boundaries. Other minor reasons may include the neglect of some details of the cask's geometry and deviation in the boundary conditions. Overall, the simulation results are acceptable and provide some insights for a thermoelectric energy harvester design.

4. Discussion and TEG design

Monitoring temperature, pressure, radiation, humidity, etc inside these enclosed vessels is crucial to ensure the reactor safe operation and fuel security. Wiring through holes in the vessel walls is undesirable and largely unfeasible in nuclear environments. To aid in this process, the development of an independent energy harvesting system to power a wireless communication system is of critical importance. Inside the enclosed spent fuel canisters, the energy source for local energy harvesting is limited, however, thermoelectric energy harvesting provide a promising solution.

To guide the design of energy harvesters for a dry cask canister, the temperature and flow velocity within the canister should be well analyzed over the lifetime of the cask. The strong convective heat transfer process inside and outside the MPC creates a large temperature drop near the canister wall, making it an ideal place for thermoelectric energy harvesting. Shown below in Fig.14 are the temperature and flow velocity profiles for years 5 and 55 (50-years dry cask storage) superimposed on each other. As can be seen, there is: one, an enduring temperature gradient present between the fuel, helium gap, and MPC wall, and two, an enduring helium circulation flow along both the wall of the fuel basket, and the wall of the MPC canister generated from convection in the helium. Using these results as a guideline, a thermoelectric energy harvester can be designed to take advantage of the existing temperature gradient here. Considering there are strong gamma radiation source within the canister, we can utilize gamma radiation by converting its energy into material heating in tungsten. The tungsten plate can create a localized hot spot. This should help to increase the temperature drop at the local site. A detailed design of the thermoelectric energy harvester for the wireless sensing and monitoring network for the canister or closed vessels will further be illustrated in a future work.

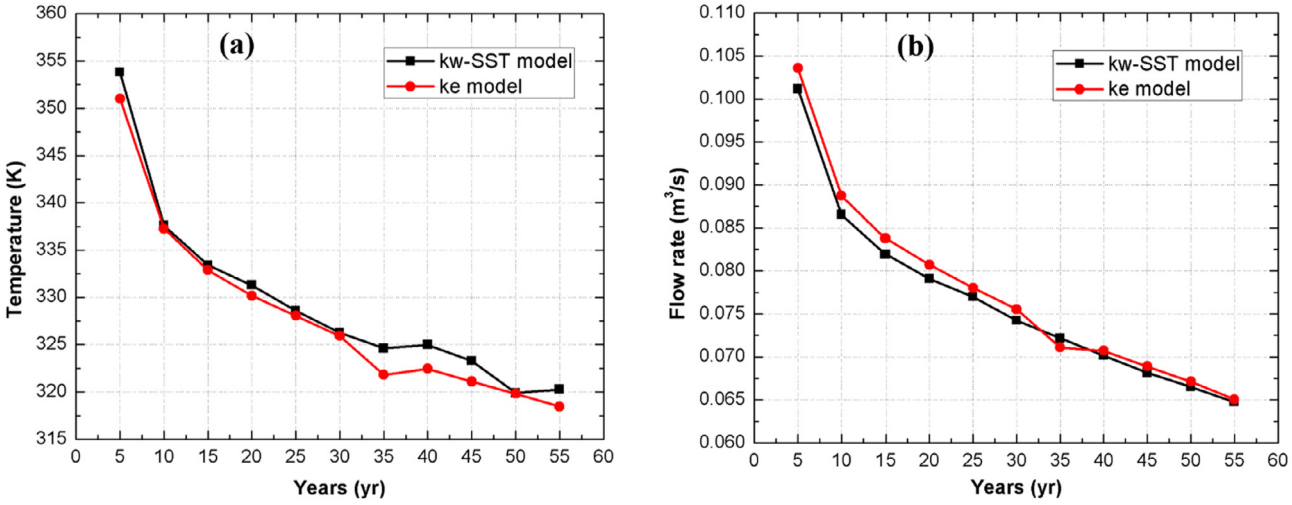

Fig. 12. (a) The flow temperature at the outlet of the air channel; (b) The flow rate at the outlet of the air channel.

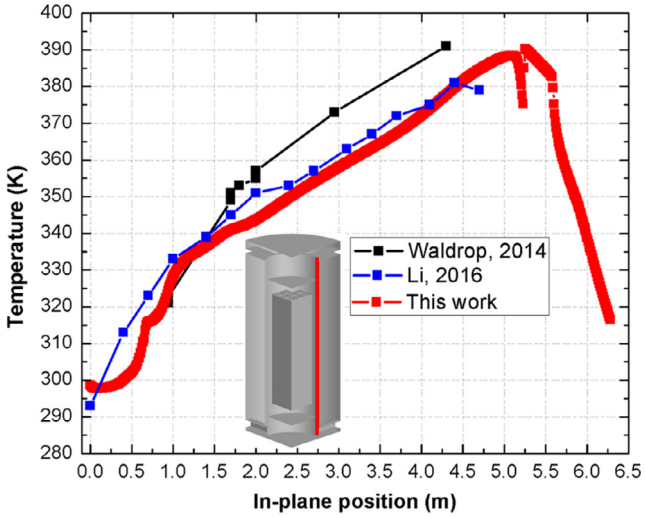

Fig. 13. The temperature profile along the outer surface of the canister.

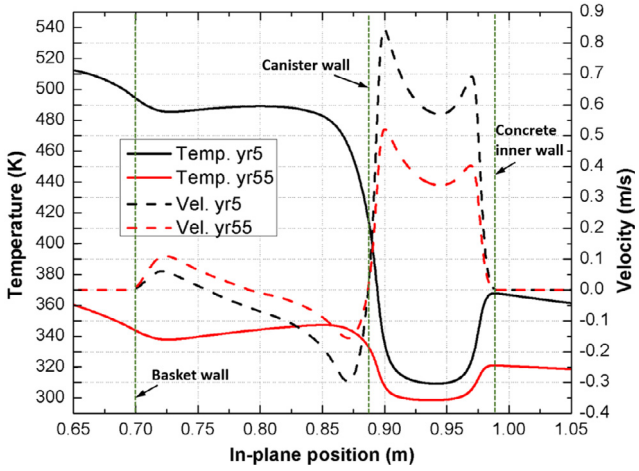

Fig. 14. The temperature and flow profiles along the center of the cask for years 5 and 55 (50 years of storage).

5. Conclusion

This paper studied the thermal-fluid behavior of a HI-STORM 100 spent fuel dry cask with a MCP-32 canister. The decay heat of the fuel was calculated from the time it enters the dry cask (5 years since removal from reactor), to 50 years in dry cask storage (55 years since removal) in intervals of 5 years using ORIGAMI. The decay heat for each specific 5-year increment was used as the input for the CFD analysis of the spent fuel cask. Some conclusions can be drawn from the results presented above:

1) In this simulation, based on some old methods and conditions well validated in previous research, several improvements were made to improve accuracy of the final results. Specifically, the decay heat was obtained from an ORIGAMI simulation of a common fuel assembly. This heat load was non-uniformly distributed in the fuel to better fit the real situation. Temperature dependent thermal properties of the air in the air channel and helium in nuclear canister were adopted along with convective heat transfer laws. To simplify the simulation, an effective thermal conductivity method was employed to simulate the anisotropic thermal conductivity of the fuel assembly.
2) The flow in the canister was in the laminar region while the flow in the air channel was in the transitional regime. Thus, the transitional SST k-ω model was more valid than the k-ε model combined with wall functions to simulate the turbulence within the air channel. Both models, however, agreed well in comparing results for both the temperature and air flow velocity at the outlet of the airflow gap in the overpack.
3) The peak temperature in each fuel assembly occurred higher in the assembly than previously assumed due to a helium gas convective cycle in the MPC driven by the buoyancy force, and had a lower value than previous calculations. This natural convection process of the helium enhanced the heat transfer inside the fuel assemblies and lowers the peak temperature within the system. The air flow through the air channel appeared to take away more than 80% of the total decay heat.
4) The heat convection and conduction outside the MPC wall effectively reduced the wall temperature, creating an ideal place for TEG placement. There was at least 30 K temperature difference available even for the worst cases, which was more than enough for a TEG energy harvester to extract tens of mW energy for the powering of a wireless sensor.

There are still several ways to improve the accuracy of the simulation results including (1) All the thermal properties should have temperature dependent values; (2) The natural convection coefficients of the concrete walls depend on the environmental temperature, thus more accurate boundary conditions are desired; (3) The grid number can be improved to get more details of the thermal-flow information within the system, which of course requires a higher computational cost; (4) The low Reynolds number k-ε model will be a better turbulence model to simulate the flow in the air channel, especially for the case with relatively low decay heat, while the laminar flow option is better to simulate the filling gas flow within the canister; (5) The emissivity of the various walls should be less than 1. Finally, an energy harvester should be designed which can effectively use the environment to self-power a wireless sensor node within the dry canister.

Acknowledgements

The authors would like to thank the DOE United States for their funding support through project number #DE-NE0008591.

References

Adkins, H.E., 2012. Modeling Used Fuel Storage Temperatures. Presentation to the US Nuclear Waste Technical Review Board.
World Nuclear Association, 2017. Nuclear Fuel and its Fabrication.
Bahney, R., Lotz, T., 1996. Spent nuclear fuel effective thermal conductivity report. Prepared for the US DOE, Yucca Mountain Site Characterization Project Office by TRW Environmental Safety Systems Inc, July 11.
Bejan, A., 2013. Convection Heat Transfer. John wiley & sons.
Brewster, R.A., Baglietto, E., Volpenhein, E., Bajwa, C.S., 2012. CFD analyses of the TN-24p PWR spent fuel storage cask, ASME 2012 Pressure Vessels and Piping Conference. Am. Soc. Mech. Eng., 17–25
Bruno, J., Ewing, R.C., 2006. Spent nuclear fuel. Elements 2, 343–349.
Carstens, T.A., 2013. Thermoelectric Powered Wireless Sensors for Dry-Cask Storage, Nuclear Engineering and Engineering Physics. University of Wisconsin-Madison.
Carstens, T.A., Corradini, M.L., Blanchard, J.P., Liu, C.-H., Li, M., Behdad, N., Ma, Z., 2013. Thermoelectric powered wireless sensors for dry-cask storage. IEEE Trans. Nucl. Sci. 60, 1072–1079.
United States Nuclear Regulatory Commission, 2017. Typical Dry Cask Storage System.
Creer, J., Michener, T., McKinnon, M., Tanner, J., Gilbert, E., Dziadosz, D., Moore, E., Schoonen, D., Jensen, M., 1987. The TN-24P PWR spent-fuel storage cask: Testing and analyses: Interim report. Pacific Northwest Lab., Richland, WA (USA); Virginia Electric and Power Co., Richmond (USA); Idaho National Engineering Lab., Idaho Falls (USA); Electric Power Research Inst., Palo Alto, CA (USA).
Das, K., Basu, D., Solis, J., Zigh, G., 2010. Computational fluid dynamics modeling approach to evaluate VSC–17 dry storage cask thermal designs, CFD for nuclear reactor safety applications. Workshop Proceedings, CFD4NRS-3, Bethesda, Maryland, USA, pp. 14-16.
Ewing, R.C., 2015. Long-term storage of spent nuclear fuel. Nat. Mater. 14, 252–257.
Greiner, M., Gangadharan, K.K., Gudipati, M., 2007. Use of fuel assembly/backfill gas effective thermal conductivities to predict basket and fuel cladding temperatures within a rail package during normal transport. Nucl. Technol. 160, 325–336.
Hedin, A., 1997. Spent nuclear fuel–how dangerous is it. SKB Report, 97-13.
Herranz, L.E., Penalva, J., Feria, F., 2015. CFD analysis of a cask for spent fuel dry storage: Model fundamentals and sensitivity studies. Ann. Nucl. Energy 76, 54–62.
Holtec International, 2004. Pressure loss characteristic for in-cell flow of helium in PWR and BWR MPC storage cells.
Holtec International, 2010. Final Safety Analysis Report for the HI-STORM 100 Cask System.
Holtec International, 2012. Final Safety Analysis Report on the Hi-Storm FW System. Holtec International.
Lee, J.C., Choi, W.S., Bang, K.S., Sea, K.S., Yoo, S.Y., 2009. Thermal-fluid flow analysis and demonstration test of a spent fuel storage system. Nucl. Eng. Des. 239, 551–558.
Li, J., Liu, Y.Y., 2016. Thermal modeling of a vertical dry storage cask for used nuclear fuel. Nucl. Eng. Des. 301, 74–88.
McKinnon, M., Dodge, R., Schmitt, R., Eslinger, L., Dineen, G., 1992. Performance testing and analyses of the VSC-17 ventilated concrete cask. Electr. Power Res. Inst.
Mittal, K., Han, Z., Li, J., Tsai, H., Liu, Y., 2014. Temperature of interest for the TN-32 cask during storage of high burnup fuel. In: INMM 55th Annual Meeting, Atlanta, Georgia, USA.
U.S. Government Accountability Office, 2017. Disposal of High-Level Nuclear Waste.
Rector, D., Cuta, J., Lombardo, N., 1986. COBRA-SFS Thermal-Hydraulic Analysis of the CASTOR-1C and REA 2023 BWR Storage Casks Containing Consolidated Spent Fuel. PNL-5802. Pacific Northwest Laboratory, Richland, Washington.
Sparrow, E.M., Azevedo, L.F.A., 1985. Vertical-channel natural-convection spanning between the fully-developed limit and the single-plate boundary-layer limit. Int. J. Heat Mass Trans. 28, 1847–1857.
Takeda, H., Wataru, M., Shirai, K., Saegusa, T., 2008. Heat removal verification tests using concrete casks under normal condition. Nucl. Eng. Des. 238, 1196–1205.
Tallackson, J., 1976. Thermal transport properties of helium, helium–air mixtures, water, and tubing steel used in the CACHE program to compute HTGR auxiliary heat exchanger performance. Oak Ridge National Lab., Tenn. (USA).
Turner, S., 1989. An Uncertainty Analysis-Axial Burnup Distribution Effects.
Versteeg, H.K., Malalasekera, W., 2007. An introduction to computational fluid dynamics: the finite volume method. Pearson Education.
Walavalkar, A.Y., Schowalter, D.G., 2004. 3-D CFD simulation of a spent nuclear fuel storage system. Trans. Am. Nucl. Soc. 91, 200–201.
Waldrop, K., Kessler, J., 2014. Update on in-service inspections of stainless steel dry storage canisters document ML14052A430 (slides), NEI-NRC Meeting on Spent Fuel Dry Storage Cask Material Degradation.
Wataru, M., Takeda, H., Shirai, K., Saegusa, T., 2008. Thermal hydraulic analysis compared with tests of full-scale concrete casks. Nucl. Eng. Des. 238, 1213–1219.
Williams, M.L., Skutnik, S.E., Gauld, I.C., Wieselquist, W.A., Lefebvre, R.A., 2015. ORIGAMI: A code for computing assembly isotopic with origen.
Xie, H., Gao, Z.Y., Zhou, Z.W., 2002. A numerical investigation of natural convection heat transfer in horizontal spent-fuel storage cask. Nucl. Eng. Des. 213, 59–65.
Yoo, S.H., No, H.C., Kim, H.M., Lee, E.H., 2010. Full-scope simulation of a dry storage cask using computational fluid dynamics. Nucl. Eng. Des. 240, 4111–4122.
Zigh, A., Solis, J., 2012. Computational Fluid Dynamics Best Practice Guidelines for Dry Cask Applications. Office of U.S. Nuclear Regulatory Research.